J. Am. Soc. Mass Spectrom. (2012) 23:2102–2114
DOI: 10.1007/s13361-012-0490-z

RESEARCH ARTICLE

Possible Evidence of Amide Bond Formation Between Sinapinic Acid and Lysine-Containing Bacterial Proteins by Matrix-Assisted Laser Desorption/Ionization (MALDI) at 355 nm

Clifton K. Fagerquist, Omar Sultan, Michelle Q. Carter

Agricultural Research Service, US Department of Agriculture, Western Regional Research Center, 800 Buchanan Street, Albany, CA 94710, USA

Abstract

We previously reported the apparent formation of matrix adducts of 3,5-dimethoxy-4-hydroxycinnamic acid (sinapinic acid or SA) via covalent attachment to disulfide bond-containing proteins (HdeA, Hde, and YbgS) from bacterial cell lysates ionized by matrix-assisted laser desorption/ionization (MALDI) time-of-flight-time-of-flight tandem mass spectrometry (TOF-TOF-MS/MS) and post-source decay (PSD). We also reported the absence of adduct formation when using α-cyano-4-hydroxycinnamic acid (CHCA) matrix. Further mass spectrometric analysis of disulfide-intact and disulfide-reduced over-expressed HdeA and HdeB proteins from lysates of gene-inserted *E. coli* plasmids suggests covalent attachment of SA occurs *not* at cysteine residues but at lysine residues. In this revised hypothesis, the attachment of SA is preceded by formation of a solid phase ammonium carboxylate salt between SA and accessible lysine residues of the protein during sample preparation under acidic conditions. Laser irradiation at 355 nm of the dried sample spot results in equilibrium retrogradation followed by nucleophilic attack by the amine group of lysine at the carbonyl group of SA and subsequent amide bond formation and loss of water. The absence of CHCA adducts suggests that the electron-withdrawing effect of the α-cyano group of this matrix may inhibit salt formation and/or amide bond formation. This revised hypothesis is supported by dissociative loss of SA (–224 Da) and the amide-bound SA (–206 Da) from SA-adducted HdeA and HdeB ions by MS/MS (PSD). It is proposed that cleavage of the amide-bound SA from the lysine side-chain occurs via rearrangement involving a pentacyclic transition state followed by hydrogen abstraction/migration and loss of 3-(4-hydroxy-3,5-dimethoxyphenyl)prop-2-ynal (–206 Da).

Key words: Ammonium carboxylate salt, MALDI, Sinapinic acid, Amide bond, Lysine residue, N-terminus, Equilibrium retrogradation, 355 nm, Bacteria, CHCA, Protein, HdeA, HdeB, Dissociative loss

Introduction

Since its inception in 1987, matrix-assisted laser desorption/ionization (MALDI) has had a dramatic impact on the science of mass spectrometry and its application to the analysis of biomolecules and other natural and synthetic compounds [1, 2]. As the number of applications utilizing

Received: 11 July 2012
Revised: 29 August 2012
Accepted: 3 September 2012
Published online: 2 October 2012

Electronic supplementary material The online version of this article (doi:10.1007/s13361-012-0490-z) contains supplementary material, which is available to authorized users.

Correspondence to: Clifton K. Fagerquist; *e-mail:* clifton.fagerquist@ars.usda.gov

MALDI increase [3–8], matrix development and selection play a significant role in optimizing this technique for a particular application [9–11]. MALDI time-of-flight mass spectrometry (TOF-MS) has become a particularly innovative technique for analysis of microorganisms [12–20]. A number of commercially available software applications have come to market that utilize pattern recognition algorithms to taxonomically "fingerprint" microorganisms from their MALDI-TOF-MS profile [21]. In addition, genomic sequence data has been linked to the mass-to-charge (*m/z*) of protein ions observed in MALDI-TOF-MS to allow a bioinformatic approach to microorganism identification [22–25].

Further development of TOF technology led to tandem TOF or TOF-TOF instruments [26, 27]. Although initially developed as a high throughput platform for bottom-up proteomics, MALDI-TOF-TOF instruments are increasingly utilized for top-down proteomic identification of non-digested proteins using either in-source decay (ISD) [28–30] or post-source decay (PSD) [31–36]. As ISD and PSD occur in different regions of the mass spectrometer there are significant differences in ion fragmentation and polypeptide backbone cleavage. MS/MS (PSD) results in lower energy fragmentation channels resulting in cleavage at the C-terminal side of aspartic acid (D) and glutamic acid (E) as well as the N-terminal side of proline (P) residues (although other cleavage sites can occur). The time from desorption/ionization to protein ion fragmentation is dependent on the amount of energy deposited into a protein during the desorption/ionization as well as any ion-molecule collisions that subsequently occur in the gas phase. Direct photon absorption by a protein in the gas phase during the laser pulse is also possible and can boost fragmentation. The most commonly used laser wavelengths are 337 nm (nitrogen) and 355 nm (third harmonic of YAG). In addition, the optical absorption characteristics of MALDI matrices vary as a function of wavelength [37, 38].

Matrix adduction to analytes is a problem that sometimes occurs with MALDI. The presence of adducts is often dependent on the chemical composition of the matrix and the analyte. A number of groups have reported adduction of MALDI matrices to disulfide containing peptides and proteins [39–42]. In an extensive study of peptides and digested proteins having disulfide bonds, Liu and coworkers were able to demonstrate covalent attachment of α-cyano-4-hydroxycinnamic acid (CHCA) (and other matrices) under disulfide reducing conditions at high pH. They proposed a base catalyzed Michael addition reaction occurring in solution with nucleophilic attack of a thio-enolate anion at the β-carbon of the CHCA matrix resulting in a mass increase of +189 Da. CHCA and α-cyano-3-hydroxycinnamic acid were found to be the most reactive matrices due to the electron withdrawing effect of the α-cyano group facilitating the reaction. Other matrices (SA, ferulic acid, and caffeic acid) were significantly less reactive under these conditions [39].

In a previous communication [42], we reported the apparent covalent attachment and dissociative loss of sinapinic acid (SA) to/from cysteine residues in disulfide bond-containing proteins (HdeA, HdeB, and YbgS) extracted from bacterial cell lysates of *E. coli* at low pH and under non-disulfide reducing conditions. Covalent attachment was assumed to occur at cysteine residues as only proteins having disulfide bonds appeared to show evidence of SA adduction. We also reported the absence of attachment or adduction when using CHCA matrix. We have conducted further MALDI-TOF-MS and MALDI-MS/MS (PSD) experiments to further examine this phenomenon using an *E. coli* strain in which *hdeA* or *hdeB* was transcribed exogenously on a plasmid under the control of an inducible promoter in order to boost expression and thus protein ion intensity by MALDI. The higher intensity of HdeA and HdeB ions (compared with ionization from lysates of wild-type *E. coli* strains [42]) reveal two types of SA adduction: covalently-bound SA as well as SA bound by electrostatic forces. MS/MS (PSD) reveals dissociative loss of both types of adduction. On the basis of these results, a revised hypothesis of SA attachment is proposed: namely that covalently-bound SA is attached by an amide bond to the side chain of lysine residues in HdeA and HdeB as a result of solid phase ammonium carboxylate salt formed during sample preparation. The intense heating and/or irradiation accompanied by the laser pulse of the dry sample spot lead to equilibrium retrogradation of the salt complex followed by nucleophilic attack of the side-chain amine of lysine at the carboxylic acid resulting in amide bond formation and loss of water (dehydration). SA bound by electrostatic forces is the ammonium carboxylate salt transferred into the gas phase. The continued lack of reactivity of CHCA in these experiments (as well as earlier experiments [42]) suggests that the electron-withdrawing effect of the α-cyano group of CHCA may inhibit ammonium carboxylate salt formation and/or amide bond formation. The previous hypothesis of covalent attachment of SA at the side-chain of cysteine residues does not appear to be correct based on these more definitive experiments.

Experimental

Construction of Escherichia coli K-12 Strain that Overexpresses HdeA or HdeB

To achieve high production of HdeA or HdeB in *E. coli*, the *hdeA* or *hdeB* gene of *E. coli* K-12 strain MG1655 (ATCC 700926) was cloned in the expression vector pBAD18 (GenBank accession number, X81838) between the restriction sites KpnI and HindIII, resulting in plasmid pXQ14 and pXQ10, respectively. The plasmids were then transformed in strain MQC203, a *hdeAB* deletion mutant of K-12 strain MG1655 [36], generating strains MQC248 and MQC238, respectively. Since the transcription of *hdeA* and *hdeB* was under control of the P_{BAD} promoter, high expression of HdeA or HdeB was achieved in the presence of the inducer arabinose.

Three 50 mL conical tubes containing 25 mL of Luria-Bertani (LB) broth were individually inoculated with frozen stock of *E. coli* (strain K-12) carrying pBAD18 plasmids with one of the following gene inserts: *hdeA* or *hdeB*. The tubes were incubated for 6 h at 37 °C (static). An aliquot of 100 µL from each suspension was then spread onto a separate LB agar plate supplemented with 50 µg/mL of carbenicillin and 0.3 %L-arabinose. The plates were incubated overnight at 37 °C.

Sample Preparation for MALDI

Samples were prepared for MALDI analysis as described previously [34–36]. Briefly, a 1 µL sterile loop was used to harvest cells from each plate after overnight culturing and transferred to an O-ring lined, 2 mL screw-cap tube containing 300 µL of extraction solution (either 300 µL water or 300 µL of 67 % water, 33 % acetonitrile and 0.2 % trifluoroacetic acid [TFA]) and ~40 mg of 0.1 mm zirconia/silica beads. All solvents were HPLC grade. The sample tube was then tightly capped and bead-beat for 1 min (Biospec Products Inc., Bartlesville, OK, USA) followed by centrifugation at 16,000*g* for 1 min.

Disulfide reduction was performed using either dithiothreitol (DTT) (Sigma, St. Louis, MO, USA) or Tri-(2-carboxyethyl)phosphine (TCEP) (G-Biosciences, St. Louis, MO, USA, cat. #786-231). For DTT reduction, 1 µL of 1 M DTT was added to 20 µL of cell lysate supernatant (water extraction), briefly vortexed, and centrifuged for 30 s at 16,000*g*. The sample was then incubated for 70 °C for

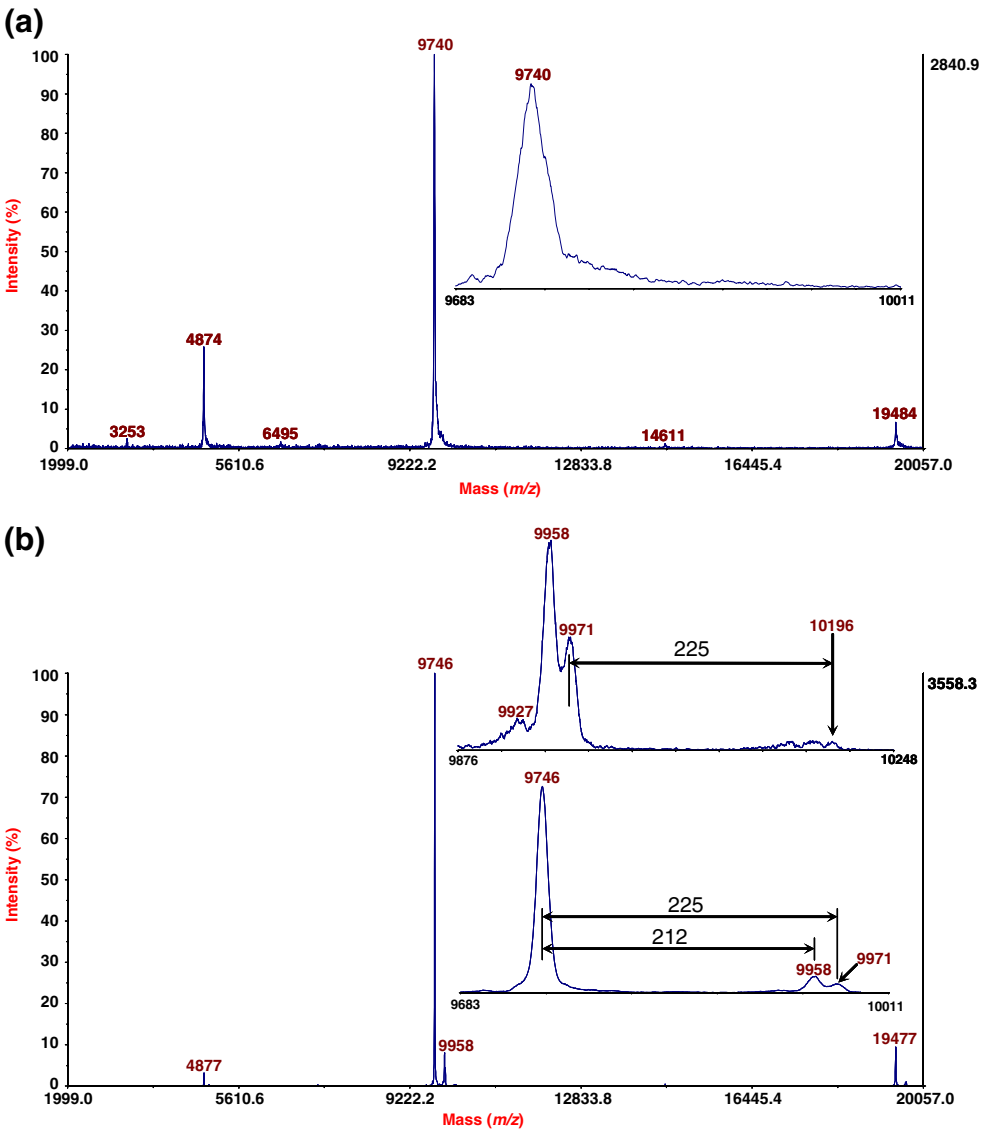

Figure 1. **(a)** MS spectrum of an unfractionated cell lysate of strain MQC248 (with HdeA) ionized with CHCA matrix. Expanded mass range is shown as insert. **(b)** MS spectrum of the same cell lysate ionized with SA matrix. Expanded mass ranges are shown as inserts

10 min, vortexed, and centrifuged for 30 s at 16,000*g*. For TCEP reduction, 0.75 μL of reductant buffer (0.5 M EDTA at pH 8) was added to 150 μL of cell lysate supernatant (water/acetonitrile/TFA extraction) and vortexed. To this solution was added 3 μL of TCEP, vortexed and incubated at room temperature for 20 min [43].

A 0.5 μL aliquot of sample supernatant was spotted onto a 384-spot stainless steel target and allowed to dry at room temperature. The dried sample spot was then overlaid with a saturated solution (67 % water, 33 % acetonitrile, and 0.2 % TFA) of either α-cyano-4-hydroxycinnamic acid (CHCA) or 3,5-dimethoxy-4-hydroxy-cinnamic acid (i.e., SA) and allowed to dry at room temperature.

Mass Spectrometry Analysis

Data was collected in MALDI-MS linear mode and MALDI-MS/MS (PSD) reflectron mode as described previously using a 4800 plus MALDI-TOF-TOF instrument (AB SCIEX, Foster City, CA, USA) [34–36]. MS linear mode was externally calibrated with a protein mixture of lysozyme, myoglobin and cytochrome-*c*. MS/MS (PSD) reflectron mode was externally calibrated with disulfide-reduced and alkylated thioredoxin [44]. Analytes were ionized using the third harmonic (355 nm) of a solid state Nd:YAG pulsed laser (18 μJ/pulse, repetition rate: 200 Hz). Laser fluence was typically in the range of 2600 to 4600 arbitrary units (AU). After a laser pulse (width: 5 ns) and a time delay, ions were accelerated from the first source at 20 kV and detected by a multi-channel plate (MCP) detector in MS linear mode. Typically, 1000 laser shots were acquired and summed in MS linear mode.

For MS/MS reflectron mode, a significantly higher laser fluence was utilized (6500 AU) during desorption/ionization in order to facilitate post-source decay (PSD). Ions were then accelerated from the first source at 8 kV. A timed ion selector (TIS) was used to isolate a pre-selected precursor ion using an acceptance window of analyte mass ±100 Da (unless otherwise noted). The isolated precursor ions were then decelerated to 1 kV before entering the collision cell. As no target gas was introduced into the collision cell, any fragmentation of the precursor ion was due to PSD. Ions were then accelerated from the second source at 15 kV. A precursor ion suppressor was used to "gate" any remaining precursor ions. Fragment ions were reflected and focused by the reflectron ion optics and detected by the reflectron MCP detector. For each MS/MS (PSD) experiment, 10 k laser shots were acquired and summed.

Raw MS data was subjected to noise filtering (correlation factor: 0.7). MS/MS (PSD) data was subjected to an advance baseline correction (peak width: 32, flexibility: 0.5, degree: 0.1) followed by noise removal (standard deviations to remove: 2) followed by Gaussian smoothing (filter width: 31 points). MS/MS (PSD) fragment ions were assigned by manual comparison to their average theoretical mass-to-charge (*m/z*) values as calculated by GPMAW ver. 8.01 a5 (Lighthouse Data, Odense, Denmark).

Results and Discussion

Figure 1a shows the MALDI-TOF-MS spectrum (as ionized using CHCA) of a unfractionated cell lysate of strain MQC248. The peak at *m/z* 9740 is the singly charged HdeA whose value is the same nominal mass to its theoretical value of *m/z* 9739.9. Figure 1b shows the MALDI-TOF-MS spectrum (ionized using SA) of the same cell lysate, which shows the HdeA ion with a *m/z* of 9746. Unlike ionization by CHCA, several satellite peaks are also observed adjacent to the HdeA peak. Inserts of expanded *m/z* ranges of these satellite ions are shown. The most prominent satellite ion is found to be 212.2 Da higher in *m/z* to that of the HdeA ion. A second less abundant ion is found to be 225.7 Da higher in *m/z* than the HdeA ion. A further *m/z* range expansion shows what appears to be multiple adduct formation.

Figure 2 shows the tandem mass spectrum (PSD) of the peak at *m/z* 9746 (HdeA) shown in Figure 1b. The high intensity of the HdeA precursor ion results in a significantly improved fragment ion intensity in contrast with our previous work analyzing a cell lysate of a wild-type *E. coli* strain [42]. Selected expanded *m/z* ranges are shown in Figure 2 as well as the amino acid sequence of HdeA (without its N-terminal signal peptide). Two cysteine residues are boxed to highlight the presence of an intramolecular disulfide bond. Asterisks inserted in the sequence denote polypeptide backbone fragmentation at that location, and the resulting b- or y-type fragment ions generated are shown above and/or below the cleavage site in the sequence. A b- or y-type ion with a ψ superscript indicates that this fragment ion is part of a fragment ion triplet resulting from cleavage of the polypeptide backbone between the two cysteine residues and symmetric and asymmetric cleavage of the disulfide bond. In addition to b- and y-type ions, we also observe single and multiple losses of ammonia (−17, −34) as well as loss of water (−18).

In Figure 2d, a curly bracket highlights fragment ion triplets. The center fragment ion of each triplet (symmetric disulfide cleavage) is identified by its corresponding b- or y-type designation. The two flanking fragment ions are shifted in mass ~± 33 Da from the center fragment ion. A sixth fragment ion triplet is centered at fragment ion y_{64} at *m/z* 7022.5 (top panel). The prominent fragment ion at *m/z* 2834.4 highlighted with an asterisk Figure 2a (insert) was not identified.

Figure 3 shows the tandem mass spectrum (PSD) of the satellite ion peaks at *m/z* 9958 and 9971 shown in Figure 1b. As the TIS gate does not have sufficient resolution to isolate these ions separately, the MS/MS (PSD) fragment ions shown could potentially be considered as originating from either (or both) of these precursor ions. Once again, expanded inserts of selected *m/z* ranges are shown in Figure 3 as well as the amino acid sequence of HdeA highlighting sites of backbone cleavage and the resulting fragment ions. The most striking observation is the appear-

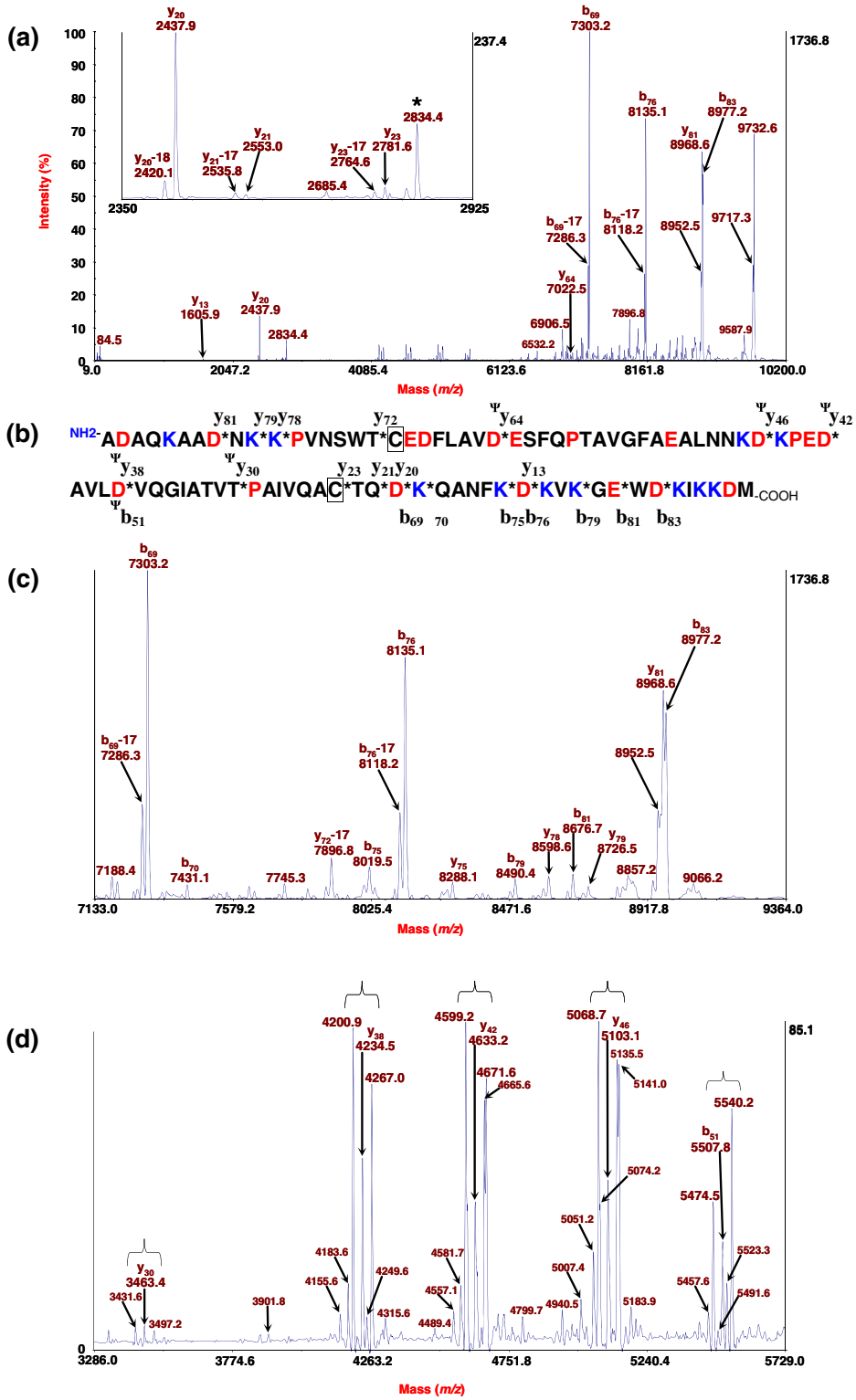

Figure 2. **(a)** MS/MS (PSD) of the disulfide-intact HdeA precursor ion at *m/z* 9746 shown in Figure 1b; **(c)**, **(d),** and insert in **(a)** are expanded *m/z* ranges of **(a)**. Fragment ions are identified by their *m/z* and their corresponding fragment ion type. A curly brackets in **(d)** designate a fragment ion triplet due to polypeptide backbone cleavage between the two cysteine residues and symmetric and asymmetric cleavage of the disulfide bond. The sequence of HdeA is provided in **(b)**. An asterisk in the sequence indicates a site of polypeptide backbone cleavage with the corresponding fragment ion type above and/or below the site of fragmentation. A ψ superscript indicates the fragment ion is part of a fragment ion triplet. The two cysteine residues that form an intramolecular disulfide bond are boxed

ance of fragment ions that are ~206 Da *and* ~224 Da higher in mass to that of a prominent fragment ion resulting from polypeptide backbone cleavage also observed in Figure 2. This would suggest that the two satellite peaks observed in Figure 1b may represent two different kinds of SA adduction to the HdeA protein: attachment of SA (M_r=224.1 Da) and attachment of SA minus a water molecule (i.e., 206.1 Da. Although the difference in *m/z* of the HdeA ion and the putative amide bound-SA-HdeA ion is *m/z* 212.2 as measured in MS linear mode [Figure 1b], this discrepancy may be due to differences in desorption velocity of the analytes, differences that are more apparent in MS linear mode than in MS/MS reflectron mode. Previously, we observed mass differences between HdeA and amide-SA-HdeA of 209 Da when ionized from lysates of wild-type *E. coli* strains [42]. Alternatively, the discrepancy could be due to *when* amide bond formation occurs. If the amide bond forms (with water loss) in the gas phase and *during* ion acceleration from the 1st source then, the mass of the amide bound-SA-HdeA ion will correspond to a value that is less than M+224 Da but more than M+206 Da. Thus, the observed mass of the amide-SA-HdeA would be affected by the time at which an amide bond is formed which is dependent on the internal energies in a population of stable and metastable SA-HdeA ions.

Beyond the additional fragment ions noted and the weaker fragment ion signal, there is a great deal of similarity between the tandem mass spectra in Figures 2 and 3. Figure 3d also shows the presence of fragment ion triplets albeit with weaker signal intensity than that found in Figure 2. The striking similarity of Figures 2 and 3 as well as the presence of fragment ion triplets in Figure 3 suggests that covalent attachment of SA to HdeA is unlikely to have occurred at either of the two cysteine residues. If it had, the fragment ion triplets would not be present in Figure 3. In consequence, the SA attachment must be occurring at another residue.

Scheme 1 outlines a possible explanation for SA attachment. Unlike our previous hypothesis of covalent attachment at the side chain of cysteine residues [42], we have concluded that the attachment is more likely to occur at the side-chain of lysine residues (and the N-terminus) as a result of formation of a solid phase ammonium carboxylate salt during the MALDI sample preparation. We propose that the rapid heating and/or dipole/electromagnetic interaction during the laser pulse result in equilibrium retrogradation of the dry salt followed by nucleophilic attack of the lysine amine at the carbonyl carbon of the SA resulting in amide bond formation with concomitant loss of water (dehydration) [45–47]. Such a mechanism was proposed for amide bond formation by microwave irradiation of neat mixtures of primary amines and carboxylic acids where it was proposed that a transition state dipole/electromagnetic interaction (i.e., a non-thermal process) was primarily responsible for facilitating amide bond formation [46]. In any case, amide bond formation by thermal heating of a carboxylic acid and an amine has been known for many years although it was found to be an inefficient reaction [47]. The low efficiency of this reaction is consistent with the relative abundances of the HdeA peak and the satellite adduct peaks in Figure 1b. HdeA has 12 lysines, and if one includes the N-terminus, there are 13 potential sites for salt/amide formation assuming all sites are accessible to the matrix. HdeB has 8 lysines, and if one includes the N-terminus, there are nine potential reaction sites. The high number of lysine residues could explain why adduction is prominent for these two proteins. We have previously detected similar adduct attachment to lysine-containing bacterial proteins (B-subunit of Shiga toxin 2 of *E. coli* and DNA binding protein HU of *Campylobacter jejuni*) when using caffeic acid (at 355 nm) and ferulic acid (at 337 nm), respectively [43, 48].

Scheme 1 also outlines mechanisms for dissociative loss of SA from HdeA and the amide-bound SA-HdeA. Electrostatic forces would allow the ammonium carboxylate salt complex to survive its transfer into the gas phase resulting in a SA-HdeA adduct ion peak ~224 Da higher in mass to that of the HdeA ion peak. Dissociative loss of the electrostatically bound SA carboxylate could occur as a result of simple equilibrium retrogradation caused by vibrational excitation. Dissociative loss of the amide-bound SA is similar to the mechanism originally proposed in our previous communication [42] (i.e., dissociative loss via formation of a pentacyclic transition state followed by hydrogen abstraction and hydrogen migration resulting in loss of 3-(4-hydroxy-3,5-dimethoxyphenyl)prop-2-ynal (−206 Da), except that it is occurring from the side-chain of a lysine (not a cysteine residue). The lack of CHCA adduction is due, presumably, to the absence of salt formation and/or amide bond formation as a result of the electron withdrawing effect of the α-cyano group. It is interesting to note that under disulfide bond-reducing conditions and at high pH in solution, CHCA is quite reactive as an adduct (in contrast to SA), and that once again the α-cyano group appears to plays critical role in determining this reactivity [39].

The mechanisms as outlined in Scheme 1 would appear to be consistent with the fragment ions observed by MS/MS (PSD) in Figures 2 and 3, which were conducted with a TIS window of ±100 Da, which was adequate resolution to exclude the more abundant HdeA ion from contributing fragment ions to the SA-HdeA MS/MS (PSD) experiment (and vice versa). However, to further eliminate any possibility of HdeA fragment ion "spillover," we conducted a series of MS/MS (PSD) experiments decreasing the TIS window (in 25 Da increments) on the lower mass side of the SA-HdeA ion peak to determine the effect, if any, on the relative abundances of fragment ions with and without attached adducts. We observed no significant variation in the relative abundances of the non-adducted versus adducted fragment ions as a function of TIS window narrowing suggesting that all fragment ions in Figure 3 originated from PSD of SA-adducted-HdeA precursor ions (Supplemental Figure 1) and not from fragment ion spillover of metastable HdeA ions.

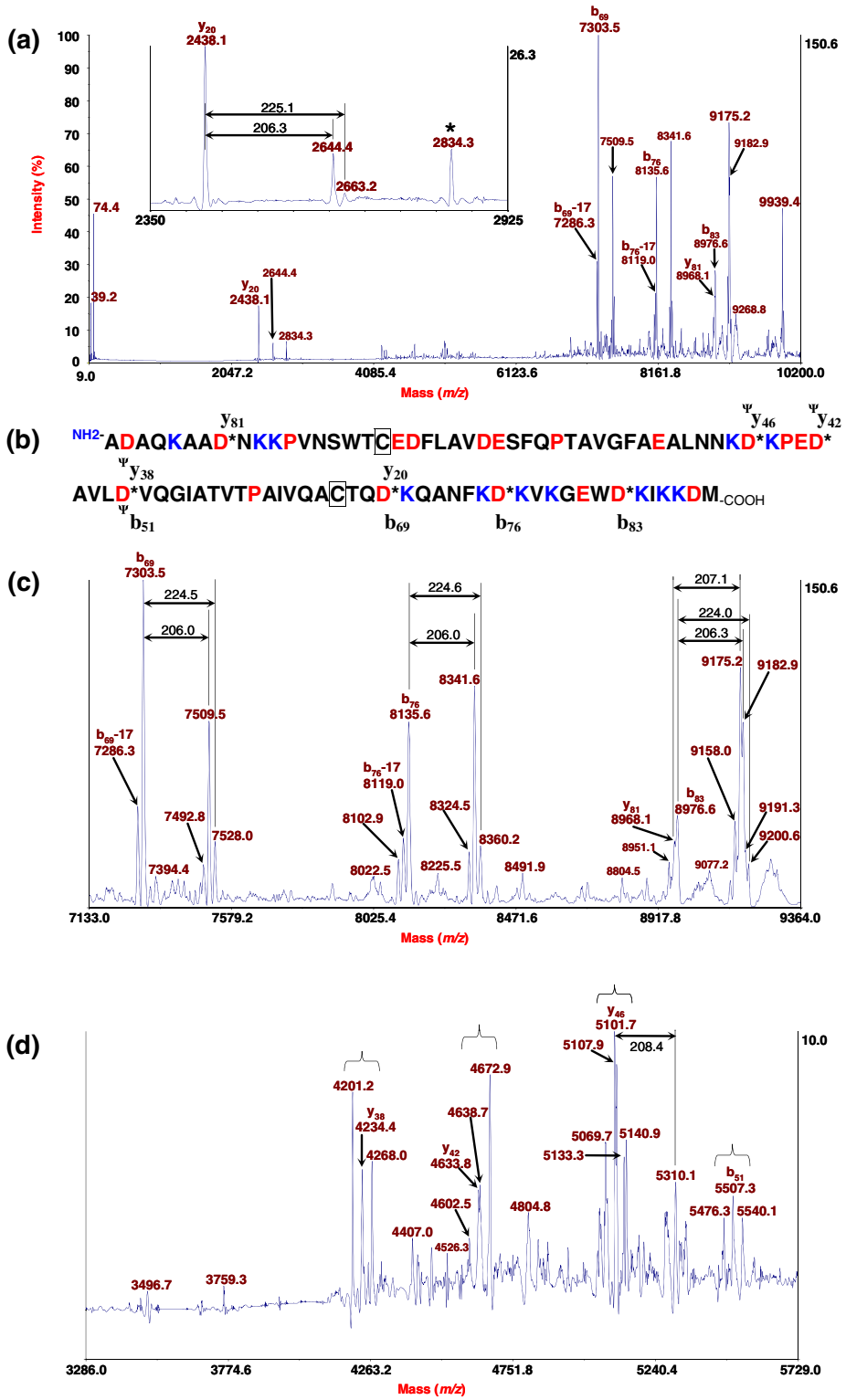

Figure 3. **(a)** Simultaneous MS/MS (PSD) of the disulfide-intact (HdeA + adducts) precursor ions at *m/z* 9958 and 9971 shown in Figure 1(b); **(c)**, **(d)**, and insert in **(a)** are expanded *m/z* ranges of **(a)**. Fragment ions are identified by their *m/z* and their corresponding fragment ion type. Additional fragment ions (not present in Figure 2) indicate adduct attachment and are highlighted by their difference in mass (or *m/z*) to the same fragment ion but without an adduct attached. A curly bracket in **(d)** designates a fragment ion triplet generated by polypeptide backbone cleavage between the two cysteine residues and symmetric and asymmetric cleavage of the disulfide bond. The sequence of HdeA is provided in **(b)**. An asterisk in the sequence indicates a site of polypeptide backbone cleavage with the corresponding fragment ion type above and/or below the cleavage site. A ψ superscript indicates the fragment ion is part of a fragment ion triplet. The two cysteine residues that form an intramolecular disulfide bond are boxed

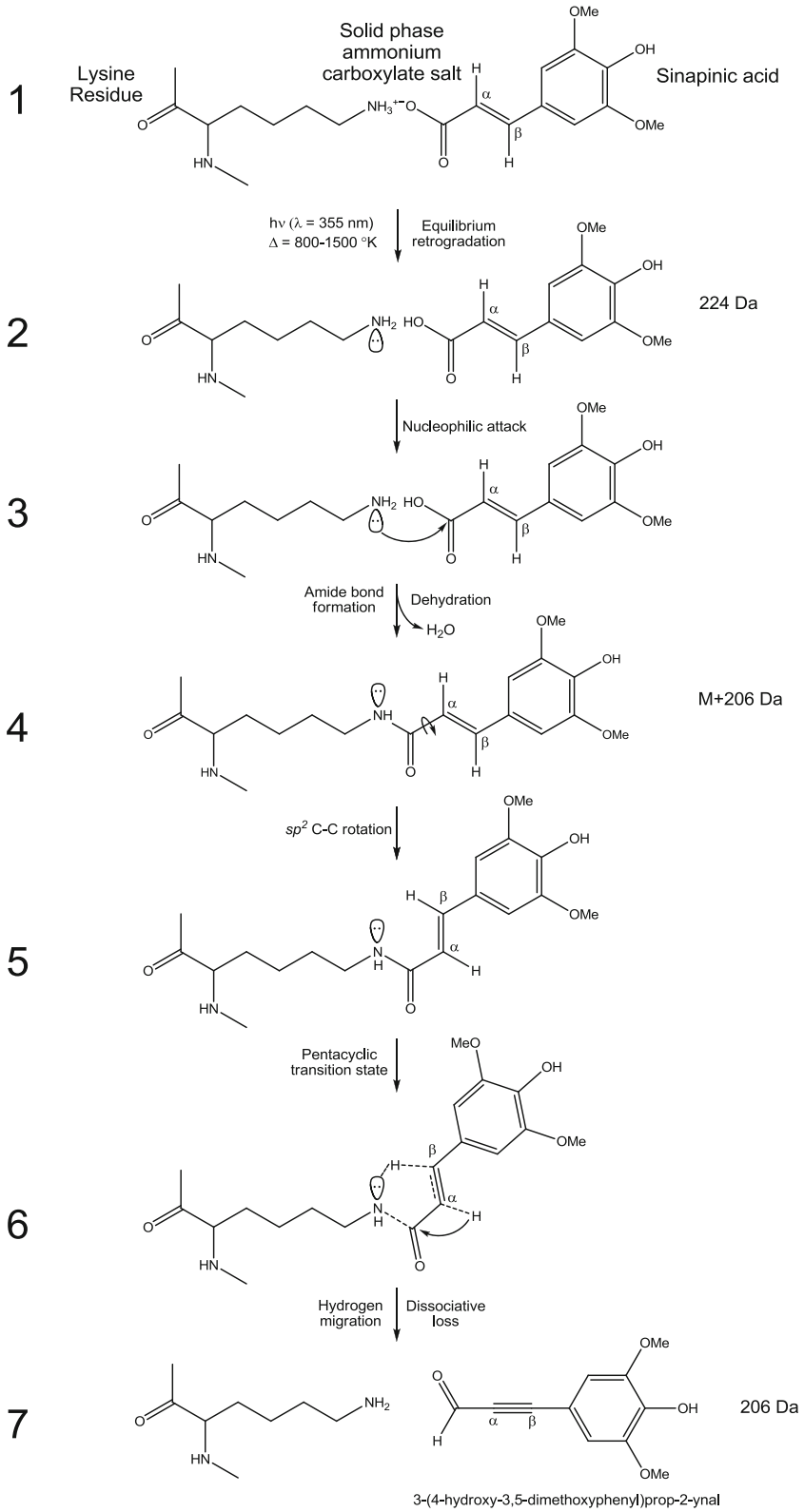

Scheme **1.** Mechanism for sinapinic acid (SA) attachment and dissociative loss at the side-chain of a lysine residue

In order to further confirm our hypothesis of SA attachment at a residue other than cysteine, the HdeA p rotein was reduced with DTT and the HdeA ion analyzed by MS/MS (PSD) shown in Figure 4. As expected, the linearized structure of disulfide-reduced HdeA results in a significantly different fragmentation pattern than that of the

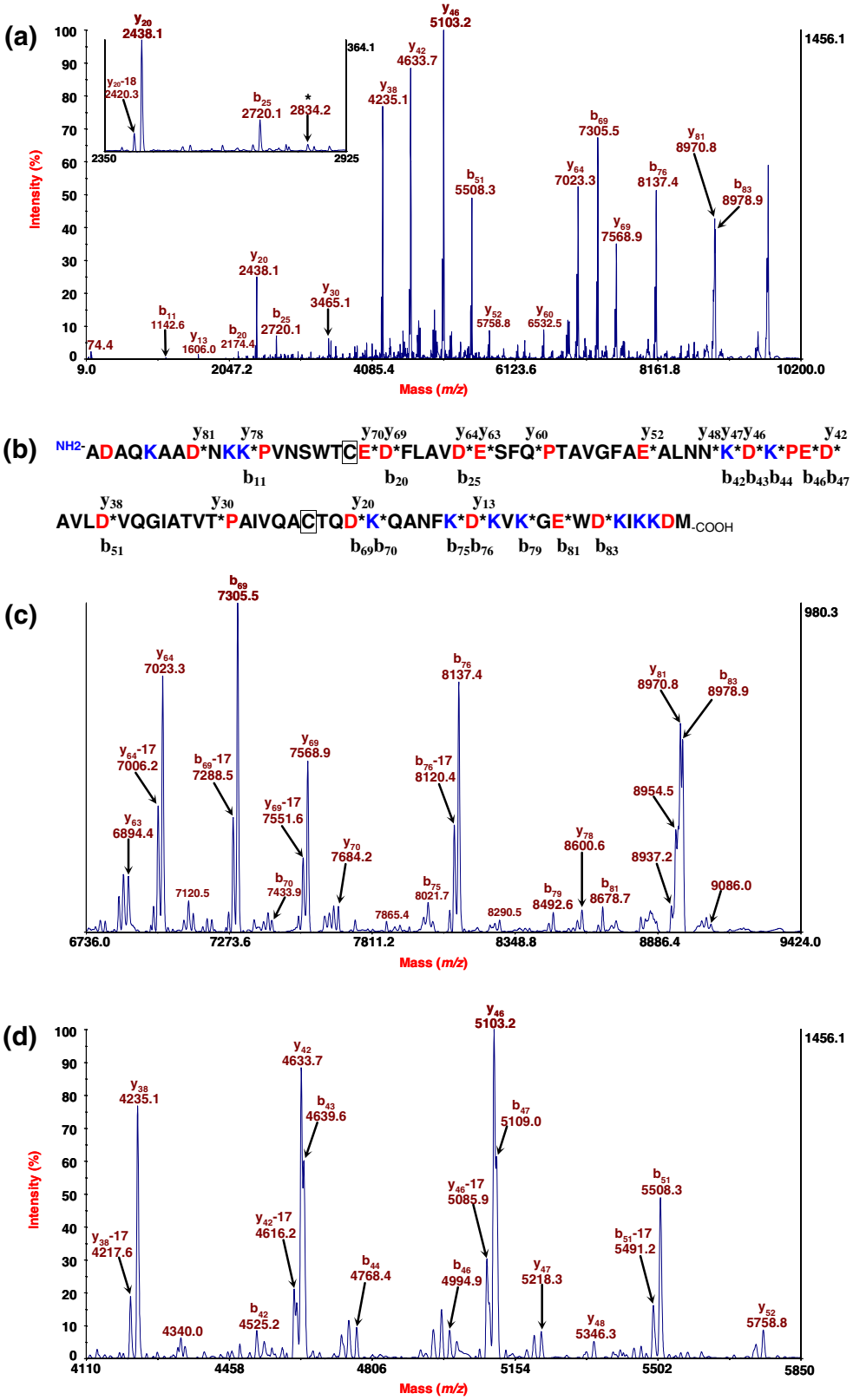

Figure 4. **(a)** MS/MS (PSD) of a disulfide-reduced HdeA precursor ion at *m/z* 9745. 4 **(c)**, **(d)**, and insert in **(a)** are expanded *m/z* ranges of **(a)**. Fragment ions are identified by their *m/z* and their corresponding fragment ion type. The sequence of HdeA is provided in **(b)**. An asterisk in the sequence indicates a site of polypeptide backbone cleavage with the corresponding fragment ion type above and/or below the cleavage site. The two cysteine residues are boxed

disulfide-intact HdeA shown in Figure 2. In particular, the flanking fragment ions of each fragment ion triplet are now absent in Figure 4, and what was previously the center fragment ion of each triplet is not only present, but dramatically increased in relative abundance compared to its abundance in the disulfide-intact HdeA tandem mass spectrum in Figure 2.

Figure 5 shows the tandem mass spectrum (PSD) of the disulfide-reduced SA-HdeA adduct ions. Once again, there is a great deal of similarity between the tandem mass spectra of the disulfide-reduced SA-HdeA precursor ion and the disulfide-reduced HdeA precursor ion shown in Figure 4. However, Figure 5 also shows additional adduct-related fragment ions (SA-HdeA and amide-bound SA-HdeA) that appear higher in mass (+224 Da and +206 Da, respectively) to that of the non-adducted fragment ions. Supplemental Figure 2 shows the effect of narrowing the TIS window on the lower mass side of the disulfide-reduced SA-HdeA precursor ions. Narrowing the TIS window had no significant effect on the relative abundance of adducted *versus* non-adducted fragment ions suggesting that fragment ion spillover from metastable HdeA was not occurring to any significant degree.

Supplemental Figure 3a shows the MALDI-TOF-MS spectrum (as ionized by CHCA) of a un-fractionated cell lysate of MQC238. The singly charged HdeB ion is shown at *m/z* 9064 whose nominal value is the same as its theoretical value of *m/z* 9064.3. Supplemental Figure 3b shows the MALDI-TOF-MS spectrum (as ionized using SA) of the same cell lysate that now shows the HdeB ion at *m/z* of 9070. Satellite ion peaks, once again, appear at ~213 and ~225 higher *m/z* to that of the HdeB ion. These satellite ion peaks do not appear when ionizing with CHCA (insert).

Supplemental Figure 4 shows MS/MS (PSD) of HdeB ionized by SA. A fairly complex fragmentation pattern is observed. Expanded *m/z* ranges are shown in Supplemental Figure 4c, d, and the insert in Supplemental Figure 4a. The HdeB amino acid sequence (without N-terminal signal peptide) is also shown in Supplemental Figure 4b with sites of polypeptide backbone cleavage designated by either a black or red asterisk with the resulting b- and/or y-type ions above and/or below the site of cleavage. A black asterisk indicates that this cleavage site results in a corresponding b- and/or y-type fragment ion(s). A red asterisk indicates that this cleavage site results in a corresponding b- and/or y-type fragment ion(s) and also fragment ions that are the result of *second* polypeptide backbone cleavage elsewhere in the sequence. Such double backbone cleavage fragment ions are observed at *m/z* 2757.6 in the insert in Supplemental Figure 4a and at *m/z* 3631.3 in Supplemental Figure 4d, and designated with their corresponding b/y ion pair. Also, it is of interest to note that these two double backbone cleavage fragment ions are also not accompanied by dissociative loss of ammonia or water unlike many single backbone cleavage fragment ions. This may be due to insufficient internal energy to undergo further dissociation after two backbone cleavages of the ion. Like HdeA, HdeB has an intramolecular disulfide bond between its two cysteine residues (boxed). A b- or y-type fragment ion with a ψ superscript indicates that this fragment ion is part of a fragment ion triplet resulting from cleavage of the polypeptide backbone between the two cysteine residues and symmetric and asymmetric cleavage of the disulfide bond. Fragment ion triplets are highlighted by a curly bracket in the spectra. The center fragment ion of each triplet (symmetric disulfide cleavage) is identified by its corresponding b- or y-type designation, and the flanking fragment ions of each triplet are ~± 33 Da from the center fragment ion. We observe an unusual number of backbone cleavages close to the cysteine near the C-terminus as shown in the insert in Supplemental Figure 4a. Concomitantly with the y_{22} fragment ion, only asymmetric cleavage of the disulfide bond (−33 Da) was observed presumably due to its proximity to the disulfide bond. A single a-type ion was assigned at *m/z* 6308.4 which is of interest because this was the only a-type fragment ion observed by MS/MS (PSD) for HdeA and HdeB.

Supplemental Figure 5 shows the tandem mass spectrum (PSD) of the putative adduct satellite ion peaks at *m/z* 9283 and, by default, *m/z* 9295 shown in Supplemental Figure 3b. The weaker signal intensity of these putative adducted HdeB ions results in a poorer MS/MS (PSD) fragment ion signal. However, we were still able to assign some of the more prominent fragment ions (i.e., b_{61}, y_{72}, and b_{76}) having no adduct and/or a SA adduct (+224 Da) and/or an amide-bound SA adduct (+206 Da).

Supplemental Figure 6 shows the effect of decreasing the TIS window (in 25 Da increments) on the low mass side of *m/z* 9283 precursor ion. As shown, we observe what appears to be some effect of TIS window narrowing on the relative intensity of fragment ions (e.g., *m/z* 6972 and *m/z* 7189), however, because of the poor MS/MS (PSD) fragment ion signal intensity, it is not clear whether this effect is indicative of fragment ion spillover from metastable HdeB ion.

Supplemental Figure 7 shows the MS/MS (PSD) disulfide-reduced HdeB ion (*m/z* 9072) ionized from a TCEP-reduced sample. Like HdeA, we observe a dramatic change in the fragmentation pattern for disulfide-reduced HdeB compared with disulfide-intact HdeB (Supplemental Figure 4). The center fragment ion of each triplet in Supplemental Figure 4 is now, in Supplemental Figure 7, the most abundant fragment ion in the spectrum which suggests the powerful effect of the disulfide bond on internal energy re-distribution and polypeptide backbone cleavage in the gas phase. The flanking fragment ions of each triplet are either eliminated or greatly reduced.

Supplemental Figure 8 shows the tandem mass spectrum (PSD) of an adduct peak at *m/z* 9284 (and by default another adduct peak at *m/z* 9297) using a TIS window of ±100 Da. Once again, we observe fragment ions without an adduct, with an amide-bound SA adduct (+206 Da) and/or a SA adduct (+224 Da).

Supplemental Figure 9 shows the effect of decreasing the TIS window (in 25 Da increments) on the low mass side of

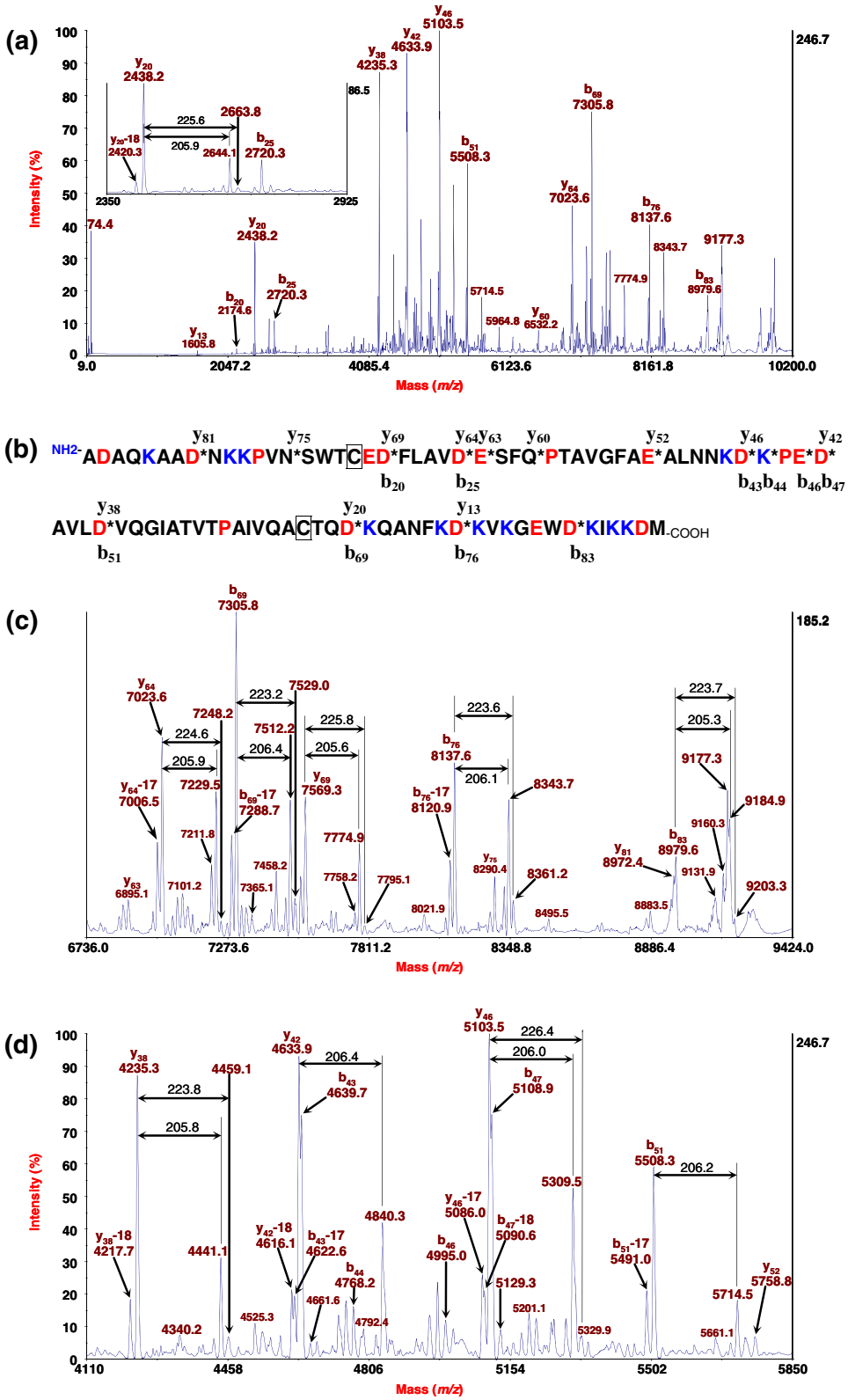

Figure 5. **(a)** Simultaneous MS/MS (PSD) of the disulfide-reduced (HdeA + adducts) precursor ions at *m/z* 9957 and *m/z* 9971; **(c)**, **(d)**, and insert in **(a)** are expanded *m/z* ranges of **(a)**. Fragment ions are identified by their *m/z* and their corresponding fragment ion type. Additional fragment ions (not present in Figure 4) indicate adduct attachment and are designated by their difference in mass (or *m/z*) to the corresponding fragment ion without an adduct. The sequence of HdeA is provided in **(b)**. An asterisk indicates a site of polypeptide backbone cleavage with the corresponding fragment ion type above and/or below the cleavage site. The two cysteine residues are boxed

the precursor ion at *m/z* 9284. We observe no effect on TIS window narrowing on the relative abundance of a fragment ion without an adduct to that of the fragment ion with an adduct suggesting that the fragment ion *sans* adduct is the result of dissociative loss from an adduct-attached precursor ion and not from fragment ion spillover from the metastable reduced HdeB ions.

Conclusions

Detailed MALDI-TOF-MS and MALDI-MS/MS (PSD) analysis of disulfide-intact and disulfide-reduced forms of HdeA and HdeB bacterial proteins ionized using CHCA and SA matrices suggest that SA is attaching at the side-chain of lysine residues (not at the side-chain of cysteine residues as previously hypothesized). The mechanism of this attachment is postulated to occur as a result of formation of a solid phase ammonium carboxylate salt during MALDI sample preparation at low pH and under disulfide bond reducing or non-reducing conditions. We postulate that rapid heating of the dry sample spot by laser irradiation at 355 nm leads to equilibrium retrogradation followed by nucleophilic attack of the lysine amine at carbonyl group of SA followed by amide bond formation and loss of water (dehydration). Dissociative loss of the amide-bound SA is postulated to occur via a pentacyclic transition state, rearrangement/fragmentation and dissociative loss of 3-(4-hydroxy-3,5-dimethoxyphenyl)prop-2-ynal (−206 Da) by a mechanism similar to that proposed earlier for dissociative loss from a cysteine residue. Dissociative loss of the electrostatically-bound SA carboxylate would occur as a result of simple equilibrium retrogradation. These gas phase dissociative mechanisms are consistent with the low energy fragmentation channels that occur by PSD. The lack of matrix adduction when using CHCA may be due to the electron-withdrawing α-cyano group disfavoring ammonium carboxylate salt formation and/or amide bond formation. Finally, expressing a gene exogenously under a strong promoter results in over-expression of the target protein and, in consequence, a strong protein ion signal by MALDI from an un-fractionated cell lysate. The strong protein ion signal results in a significant improvement in identification of MS/MS (PSD) fragment ions. By this approach, we were able to identify many more of the less-abundant fragment ions including fragment ion triplets, multiple losses of water and/or ammonia, as well as fragment ions resulting from double cleavage of the polypeptide backbone.

Acknowledgments

The authors are grateful to Jacqueline W. Louie for assistance in microbiology and plasmid development. This work was supported by USDA-ARS CRIS project 5325-42000-047-00D. USDA is an equal opportunity provider and employer.

Mention of a brand or firm name does not constitute an endorsement by the US Department of Agriculture over other of a similar nature not mentioned. This article is a US Government work and is in the public domain in the United States of America.

References

1. Karas, M., Bachmann, D., Bahr, U., Hillenkamp, F.: Matrix-assisted ultraviolet laser desorption of non-volatile compounds. *Int. J. Mass Spectrom. Ion Processes* **78**, 53–68 (1987)
2. Tanaka, K., Ido Y., Akita S., Yoshida Y., Yoshida T.: Detection of high mass molecules by laser desorption time-of-flight mass spectrometry. *Proceedings of the 2nd Japan–China Joint Symposium on Mass Spectrometry.* Osaka, Japan, Abstract 185–188 (1987)
3. Wu, K.J., Odom, R.W.: Characterizing synthetic polymers by MALDI MS. *Anal. Chem.* **70**, 456A–461A (1998)
4. Zucht, H.D., Lamerz, J., Khamenia, V., Schiller, C., Appel, A., Tammen, H., Crameri, R., Selle, H.: Data-mining methodology for LC-MALDI-MS based peptide profiling. *Comb. Chem. High Throughput Screen.* **8**, 717–723 (2005)
5. Chaurand, P., Norris, J.L., Cornett, D.S., Mobley, J.A., Caprioli, R.M.: New developments in profiling and imaging of proteins from tissue sections by MALDI mass spectrometry. *J Proteome Res.* **5**, 2889–2900 (2006)
6. Fenselau, C., Demirev, P.A.: Characterization of intact microorganisms by MALDI mass spectrometry. *Mass Spectrom Rev.* **20**, 157–171 (2001)
7. Lay, J.O. Jr.: MALDI-TOF mass spectrometry of bacteria. *Mass Spectrom. Rev*. **20**, 172–194 (2001)
8. Demirev, P.A., Fenselau, C.: Mass spectrometry in biodefense. *J. Mass Spectrom*. **43**, 1441–1457 (2008)
9. Ulmer, L.A., Mattay, J.A., Torres-Garcia, H.G.B., Luftmann, H.C.: The use of 2-[(2E)-3-(4-tert-butylphenyl)-2-methylprop-2-enylidene]malononitrile as a matrix for matrix-assisted laser desorption/ionization mass spectrometry. *Eur. J. Mass Spectrom.* **6**, 49–52 (2000)
10. Lou, X., de Waal, B.F., van Dongen, J.L., Vekemans, J.A., Meijer, E.W.: A pitfall of using 2-[(2E)-3-(4-tert-butylphenyl)-2-methylprop-2-enylidene]malononitrile as a matrix in MALDI TOF MS: chemical adduction of matrix to analyte amino groups. *J. Mass Spectrom.* **45**, 1195–1202 (2010)
11. Fenaille, F., Tabet, J.C., Guy, P.A.: Identification of 4-hydroxy-2-nonenal-modified peptides within unfractionated digests using matrix-assisted laser desorption/ionization time-of-flight mass spectrometry. *Anal. Chem.* **76**, 867–873 (2004)
12. Claydon, M.A., Davey, S.N., Edwards-Jones, V., Gordon, D.B.: The rapid identification of intact microorganisms using mass spectrometry. *Nat. Biotechnol.* **14**, 1584–1586 (1996)
13. Krishnamurthy, T., Ross, P.L., Rajamani, U.: Detection of pathogenic and non-pathogenic bacteria by matrix-assisted laser desorption/ionization time-of-flight mass spectrometry. *Rapid Commun. Mass Spectrom.* **10**, 883–888 (1996)
14. Holland, R.D., Wilkes, J.G., Rafii, F., Sutherland, J.B., Persons, C.C., Voorhees, K.J., Lay Jr., J.O.: Rapid identification of intact whole bacteria based on spectral patterns using matrix-assisted laser desorption/ionization with time-of-flight mass spectrometry. *Rapid Commun. Mass Spectrom.* **10**, 1227–1232 (1996)
15. Arnold, R., Reilly, J.: Fingerprint matching of *E. coli* strains with matrix-assisted laser desorption/ionization time-of-flight mass spectrometry of whole cells using a modified correlation approach. *Rapid Commun. Mass Spectrom* **12**, 630–636 (1998)
16. Welham, K., Domin, M., Scannell, D., Cohen, E., Ashton, D.: The characterization of micro-organisms by matrix-assisted laser desorption/ionization time-of-flight mass spectrometry. *Rapid Commun. Mass Spectrom.* **12**, 176–180 (1998)
17. Wang, Z., Russon, L., Li, L., Roser, D., Long, S.R.: Investigation of spectral reproducibility in direct analysis of bacteria proteins by matrix-assisted laser desorption/ionization time-of-flight mass spectrometry. *Rapid Commun. Mass Spectrom.* **12**, 456–464 (1998)
18. Ramirez, J., Fenselau, C.: Factors contributing to peak broadening and mass accuracy in the characterization of intact spores using matrix-assisted laser desorption/ionization coupled with time-of-flight mass spectrometry. *J. Mass Spectrom.* **36**, 929–936 (2001)

19. Wahl, K.L., Wunschel, S.C., Jarman, K.H., Valentine, N.B., Petersen, C.E., Kingsley, M.T., Zartolas, K.A., Saenz, A.J.: Analysis of microbial mixtures by matrix-assisted laser desorption/ionization time-of-flight mass spectrometry. *Anal. Chem.* **74**, 6191–6199 (2002)
20. Wunschel, S.C., Jarman, K.H., Petersen, C.E., Valentine, N.B., Wahl, K.L., Schauki, D., Jackman, J., Nelson, C.P., White, E.V.: Bacterial analysis by MALDI-TOF mass spectrometry: an inter-laboratory comparison. *J. Am. Soc. Mass Spectrom.* **16**, 456–462 (2005)
21. Carbonnelle, E., Grohs, P., Jacquier, H., Day, N., Tenza, S., Dewailly, A., Vissouarn, O., Rottman, M., Herrmann, J.L., Podglajen, I., Raskine, L.: Robustness of two MALDI-TOF mass spectrometry systems for bacterial identification. *J. Microbiol. Methods* **89**, 133–136 (2012)
22. Demirev, P.A., Ho, Y.-P., Ryzhov, V., Fenselau, C.: Microorganism identification by mass spectrometry and protein database searches. *Anal. Chem.* **71**, 2732–2738 (1999)
23. Peneda, F.J., Lin, J.S., Fenselau, C., Demirev, P.A.: Testing the significance of microorganism identification by mass spectrometry and proteome database search. *Anal. Chem.* **72**, 3739–3744 (2000)
24. Demirev, P.A., Lin, J.S., Peneda, F.J., Fenselau, C.: Bioinformatics and mass spectrometry for microorganism identification: proteome-wide post-translational modifications and database search algorithms for characterization of intact H. pylori. *Anal. Chem* **73**, 4566–4573 (2001)
25. Peneda, F.J., Antoine, M.D., Demirev, P.A., Feldman, A.B., Jackman, J., Longenecker, M., Lin, J.S.: Microorganism identification by matrix-assisted laser/desorption ionization mass spectrometry and model-derived ribosomal protein biomarkers. *Anal. Chem.* **75**, 3817–3822 (2003)
26. Medzihradszky, K.F., Campbell, J.M., Baldwin, M.A., Falick, A.M., Juhasz, P., Vestal, M.L., Burlingame, A.L.: The characteristics of peptide collision-induced dissociation using a high-performance MALDI-TOF/TOF tandem mass spectrometer. *Anal. Chem.* **72**, 552–558 (2000)
27. Suckau, D., Resemann, A., Schuerenberg, M., Hufnagel, P., Franzen, J., Holle, A.: A novel MALDI LIFT-TOF/TOF mass spectrometer for proteomics. *Anal. Bioanal. Chem.* **376**, 952–965 (2003)
28. Suckau, D.A., Resemann, A.: T3-sequencing: targeted characterization of the N- and C-termini of undigested proteins by mass spectrometry. *Anal Chem.* **75**, 5817–5824 (2003)
29. Hardouin, J.: Protein sequence information by matrix-assisted laser desorption/ionization in-source decay mass spectrometry. *Mass Spectrom Rev.* **26**, 672 (2007)
30. Calligaris, D., Villard, C., Terras, L., Braguer, D., Verdier-Pinard, P., Lafitte, D.: MALDI in-source decay of high mass protein isoforms: application to alpha- and beta-tubulin variants. *Anal Chem.* **82**, 6176–6184 (2010)
31. Lin, M., Campbell, J.M., Mueller, D.R., Wirth, U.: Intact protein analysis by matrix-assisted laser desorption/ionization tandem time-of-flight mass spectrometry. *Rapid Commun. Mass Spectrom.* **17**, 1809–1814 (2003)
32. Demirev, P.A., Feldman, A.B., Kowalski, P., Lin, J.S.: Top-down proteomics for rapid identification of intact microorganisms. *Anal. Chem.* **77**, 7455–7461 (2005)
33. Liu, Z., Schey, K.L.: Fragmentation of multiply-charged intact protein ions using MALDI-TOF-TOF mass spectrometry. *J. Am. Soc. Mass Spectrom.* **19**, 231–238 (2008)
34. Fagerquist, C.K., Garbus, B.R., Williams, K.E., Bates, A.H., Boyle, S., Harden, L.A.: Web-based software for rapid top-down proteomic identification of protein biomarkers, with implications for bacterial identification. *Appl. Environ. Microbiol.* **75**, 4341–4353 (2009)
35. Fagerquist, C.K., Garbus, B.R., Miller, W.G., Williams, K.E., Yee, E., Bates, A.H., Boyle, S., Harden, L.A., Cooley, M.B., Mandrell, R.E.: Rapid identification of protein biomarkers of *Escherichia coli* O157:H7 by matrix-assisted laser desorption ionization-time-of-flight-time-of-flight mass spectrometry and top-down proteomics. *Anal. Chem.* **82**, 2717–2725 (2010)
36. Carter, M.Q., Louie, J.W., Fagerquist, C.K., Sultan, O., Miller, W.G., Mandrell, R.E.: Evolutionary silence of the acid chaperone protein HdeB in enterohemorrhagic *Escherichia coli* O157:H7. *Appl. Environ. Microbiol.* **78**, 1004–1014 (2012)
37. Allwood, D.A., Dreyfus, R.W., Perera, I.K., Dyer, P.E.: UV optical absorption of matrices used for matrix-assisted laser desorption/ionization. *Rapid Commun. Mass Spectrom.* **10**, 1575–1578 (1996)
38. Low, W., Kang, J., DiGruccio, M., Kirby, D., Perrin, M., Fischer, W.H.: MALDI-MS analysis of peptides modified with photolabile arylazido groups. *J. Am. Soc. Mass Spectrom.* **15**, 1156–1160 (2004)
39. Yang, H., Liu, N., Qiu, X., Liu, S.: A new method for analysis of disulfide-containing proteins by matrix-assisted laser desorption ionization (MALDI) mass spectrometry. *J. Am. Soc. Mass Spectrom.* **20**, 2284–2293 (2009)
40. Happersberger, H.P., Bantscheff, M., Barbirz, S., Glocker, M.O.: Multiple and subsequent MALDI-MS on-target chemical reactions for the characterization of disulfide bonds and primary structures of proteins. *Methods Mol. Biol.* **146**, 167–184 (2000)
41. Spiess, C., Happersberger, H.P., Glocker, M.O., Spiess, E., Rippe, K., Ehrmann, M.: Biochemical characterization and mass spectrometric disulfide bond mapping of periplasmic alpha-amylase MalS of *Escherichia coli*. *J. Biol. Chem.* **272**, 22125–22133 (1997)
42. Fagerquist, C.K., Garbus, B.R., Williams, K.E., Bates, A.H., Harden, L.A.: Covalent attachment and dissociative loss of sinapinic acid to/from cysteine-containing proteins from bacterial cell lysates analyzed by MALDI-TOF-TOF mass spectrometry. *J. Am. Soc. Mass Spectrom.* **21**, 819–832 (2010)
43. Fagerquist, C.K., Sultan, O.: Induction and identification of disulfide-intact and disulfide-reduced β-subunit of Shiga toxin 2 from *Escherichia coli* O157:H7 using MALDI-TOF-TOF-MS/MS and top-down proteomics. *Analyst* **136**, 1739–1746 (2011)
44. Fagerquist, C.K., Sultan, O.: A new calibrant for matrix-assisted laser desorption/ionization time-of-flight-time-of-flight post-source decay tandem mass spectrometry of non-digested proteins for top-down proteomic analysis. *Rapid Commun. Mass Spectrom.* **26**, 1241–1248 (2012)
45. Charville, H., Jackson, D., Hodges, G., Whiting, A.: The thermal and boron-catalyzed direct amide formation reactions: mechanistically understudied yet important processes. *Chem Commun.* **46**, 1813–1823 (2010)
46. Perreux, L.A., Loupy, A.A., Volatron, F.B.: Solvent-free preparation of amides from acids and primary amines under microwave irradiation. *Tetrahedron* **58**, 2155–2162 (2002)
47. Mitchell, J.A., Reid, E.E.: The preparation of aliphatic amides. *J. Am. Chem. Soc.* **53**, 1879–1883 (1931)
48. Fagerquist, C.K., Miller, W.G., Harden, L.A., Bates, A.H., Vensel, W.H., Wang, G., Mandrell, R.E.: Genomic and proteomic identification of a DNA-binding protein used in the "fingerprinting" of campylobacter species and strains by MALDI-TOF-MS protein biomarker analysis. *Anal. Chem.* **77**, 4897–4907 (2005)